

Reactions of Gas-Phase Atomic Hydrogen with Chemisorbed Hydrogen on a Graphite Surface

Jongbaik Ree,* Yoo Hang Kim,[†] and Hyung Kyu Shin[‡]

Department of Chemistry Education, Chonnam National University, Gwangju 500-757, Korea. *E-mail: jbreed@chonnam.ac.kr

[†]Department of Chemistry and Center for Chemical Dynamics, Inha University, Incheon 402-751, Korea

[‡]Department of Chemistry, University of Nevada, Reno, Nevada 89557, U.S.A.

Received January 23, 2007

The reaction of gas-phase hydrogen atoms H with H atoms chemisorbed on a graphite surface has been studied by the classical dynamics. The graphite surface is composed of the surface and 10 inner layers at various gas and surface temperatures (T_g , T_s). Three chains in the surface layer and 13 chains through the inner layers are considered to surround the adatom site. Four reaction pathways are found: H₂ formation, H-H exchange, H desorption, and H adsorption. At (1500 K, 300 K), the probabilities of H₂ formation and H desorption are 0.28 and 0.24, respectively, whereas those of the other two pathways are in the order of 10⁻². Half the reaction energy deposits in the vibrational motion of H₂, thus leading to a highly excited state. The majority of the H₂ formation results from the chemisorption-type H(g)-surface interaction. Vibrational excitation is found to be strong for H₂ formed on a cold surface (~10 K), exhibiting a pronounced vibrational population inversion. Over the temperature range (10-100 K, 10 K), the probabilities of H₂ formation and H-H exchange vary from 0 to ~0.1, but the other two probabilities are in the order of 10⁻³.

Key Words : Collision-induced, Graphite, Hydrogen, Chemisorbed, Recombination

Introduction

The gas atoms incident on the surface can cause the dissociation of adatoms from the surface sites. The desorbing atom can combine with the gas atom, thus forming a diatomic molecule in a highly exothermic reaction, or recede from the surface without reacting with the gas atom. The energy of the bond formed between the atoms typically lies between 4 and 5 eV,¹ whereas the chemisorption energy is significantly lower.²⁻⁴ For example, the oxygen-to-platinum adsorption energy is 0.52 eV² and the hydrogen-to-graphite adsorption energy is ~0.6 eV.⁴ Although the hydrogen adsorption energies for other non-metal as well as metal surfaces are known to be significantly higher (e.g., 3.5 eV for H/Si,^{5,6} 3.0 eV for H/Ni,^{7,8} and 2.3 eV for H/W,⁹), the differences between the bond and chemisorption energies are often large, suggesting that when the atoms combine in such cases, a large amount of energy can be liberated. As a consequence of energy conservation the released energy deposits in various degrees of freedom of the final product.

The H(ad)/C(gr) system is a prototype model in understanding details of gas-surface reactions due to its favorable characteristics for an incident gas-phase H atom to be attracted for reactive events. In this system, the exoergicity of the H₂ formation can be as large as 4 eV. Even though the product is a simple diatomic molecule, the H₂ formation on a surface is complicated by the participation of various competing reaction pathways, many-body interactions, surface relaxation and surface characteristics, thus offering many challenging problems.^{4,10-19} Although only two simple atoms and an adatom site are involved in the reaction zone, the actual reaction pathways might be complicated, since H(g)

interacts not only with H(ad) but also with many surface sites nearby the adatom site, which are coupled to the adjacent carbon atoms in the surface layers as well as the inner chain atoms and finally to the bulk phase. The effects of many-body interactions make this and related gas-surface reactions radically different from gas-phase reactions. The collection of the adatom sites and all nearby carbon atoms act as a third body in the H₂ formation, *i.e.*, the reaction takes place on a tiny surface site of the solid block composed of a large number of carbon atoms compared to a simple three-body interaction in the gas phase. Another important aspect is that the surface carbon atoms distributed around the adatom site can direct the incident gas atoms approaching the surface at large impact parameters towards the adatom so that the recombination can occur. There is no comparable role played by the third body in a gas phase recombination reaction.^{20,21} The H₂ formation results when the adatom-surface bond is violently disturbed in a short time scale. The system can produce energy deposit in specific modes in such a time scale and maintain it in them as the product molecule recedes from the surface. For example, vibrational excitation can be deduced from the dynamical information. Energy transfer from the reaction site to the solid can be much slower than the time scale for the build-up of energy in H₂, thus requiring a procedure different from that for the bond formation to describe surface energy relaxation.²² Details of energy flow between various motions and formation of nascent bonds in the collision-induced process can be understood by studying the time evolution of collision trajectories during the collision and not by the asymptotic trajectories. If products are thermalized on the surface, no such information can be obtained.

It has been proposed that interstellar grains are a collection of small particles of silicates, amorphous carbon, and graphite bonded together into a loose aggregate.²³⁻²⁵ Since atomic hydrogen is by far the most abundant gaseous species in the interstellar medium at extreme temperatures (10 K), the problem of studying rates and mechanisms of the H(g)/C(gr) reaction is then both interesting and important in understanding some astrophysical phenomena, such as the infrared emission of the interstellar clouds.^{18,26} Therefore, the information on the amount of reaction energy deposited in the various motions of the nascent hydrogen molecule, especially its vibrational population distribution, should be particularly useful in understanding the infrared emission.

In this paper, we study the collision of a gas-phase H atom with an H atom chemisorbed on a graphite surface. The surface consists of the center site on which H(ad) is chemisorbed surrounded by 12 first-, second-, and third-nearest atoms, a three benzene ring C₁₃ structure. These surface layer atoms extend infinitely. These atoms are also coupled to the bulk phase through inter-layer chains. Our main objective is to study the dynamics of the recombination reaction $\text{H(g)} + \text{H(ad)/C(gr)} \rightarrow \text{H}_2\text{(g)} + \text{C(gr)}$ and explore the participation of other reaction pathways. Particular emphases will be placed on the time evolution of reactive events, temperature dependence of reaction probabilities and distribution of energy released in the reaction among various motions of the product in an extensive surface environment, where energy propagates into the bulk surface and the carbon atoms remote from the adatom site can also affect the recombination. The H(g)-surface interaction can lead to other pathways, such as H-H exchange reaction, collision-induced desorption of H(ad) without forming H₂(g), and adsorption of H(g) on one of the nearby sites also without

forming H₂(g), which will also be studied here. The problem of the participation of H(g)-adjacent carbon atom interactions, which has been encountered in other studies mentioned above, can lead to a number of new effects on the gas-surface reaction; namely, the adsorption of H(g) on one of the adjacent carbon atoms opening up a new reaction pathway, steering of H(g) towards or away from H(ad) by the atoms, and propagation of the reaction energy to the remote region of the surface layer. The incident atom approaching the surface at a large impact parameter will be strongly influenced by adjacent surface sites, which can steer H(g) towards the reaction site. We consider this problem to be particularly important in understanding the mechanism of gas-surface reactions and it can best be treated when there is only one adatom in the region of influence, *i.e.*, a sparsely adsorbed system, thus eliminating complications to the steering effect coming from other adatoms. An important part of the computational procedures is to determine the time evolution of the entire interaction system by solving the equations of motion of all atoms involved. The study is devoted to the collisions taking place at a higher temperature condition, where the gas temperature $T_g = 1500$ K and the surface temperature $T_s = 300$ K, and at a low temperature condition, where $T_g = 10$ -100 K and $T_s = 10$ K, mimicking the interstellar environment.

Model

The model of the interaction of atomic hydrogen H(g) with chemisorbed hydrogen H(ad) on a graphite surface is shown in Figure 1a. The adatom is adsorbed on the center atom C₍₀₎ of a planar surface, a chemisorption site, which is surrounded by many surface-layer C atoms. The first-nearest

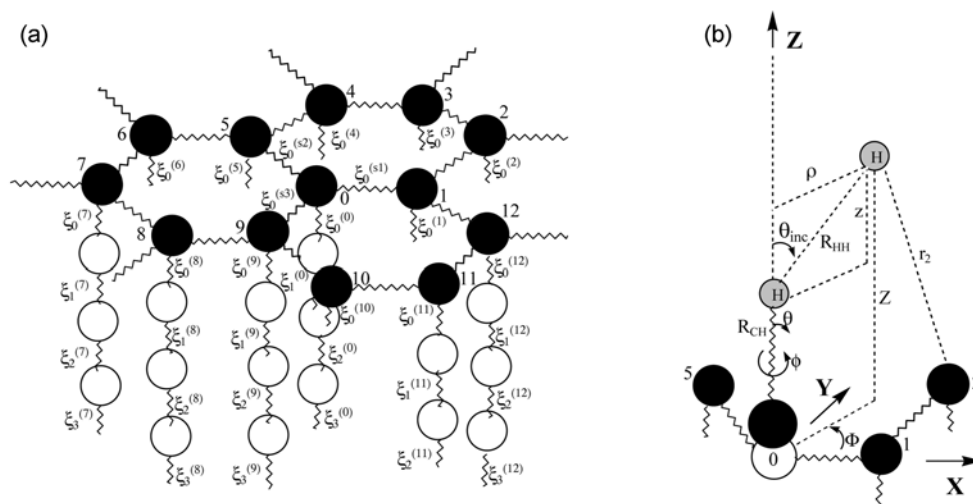


Figure 1. Interaction model. For a clearer presentation, the graphite phase and reaction zone are separated. (a) Graphite phase: the surface-layer (s1, s2 and s3) and inner-layer chains (0, 1, 2, ..., 12) are shown. Each chain has $N+1=11$ atoms. For clarity, only the first several atoms of each chain are indicated. The N th carbon atom is bound to the bulk phase. (b) The reaction-zone atoms, H(g), H(ad) and C₍₀₎ are shown. The adatom is on C₍₀₎ which is puckered from the basal plane. For convenience C₍₁₎, C₍₂₎ and C₍₅₎, as well as the H(g)-to-C₍₂₎ distance r_2 are shown. The position of the unpuckered C₍₀₎ indicated by an open circle is the origin of the XYZ coordinate system. From this position to C₍₁₎ is the direction of the X axis. The coordinate system (R_{CH} , θ , ϕ) describes the instantaneous position of H(ad), θ being the rotational angle from the Z axis and ϕ being the azimuthal angle.

atoms from $C_{(0)}$ are $C_{(1)}$, $C_{(5)}$ and $C_{(9)}$, the second-nearest neighbors are $C_{(2)}$, $C_{(4)}$, $C_{(6)}$, $C_{(8)}$, $C_{(10)}$ and $C_{(12)}$, and the third-nearest neighbors are $C_{(3)}$, $C_{(7)}$ and $C_{(11)}$. Three chains $s1$, $s2$ and $s3$ begin from $C_{(0)}$ in sideways in the surface layer, and their initial bonds link $C_{(0)}$ to $C_{(1)}$, $C_{(0)}$ to $C_{(5)}$ and $C_{(0)}$ to $C_{(9)}$, respectively. Two chains branch out from each of $C_{(1)}$, $C_{(5)}$ and $C_{(9)}$, e.g., $C_{(1)}$ to $C_{(2)}$ and $C_{(1)}$ to $C_{(12)}$. These three chains eventually branch out to a large number of tributary chains, which eventually bind to the bulk phase; i.e., the sequence of each chain is 0, 1, ..., N , where we consider atoms beyond the N th atom belong to the bulk phase.

In Figure 1a, the vibration of each carbon atom is represented by $\xi_j^{(i)}$ for the j th atom of the i th chain. For the 13 surface-layer (i.e., 0th layer) atoms, we then have $\xi_0^{(0)}$, $\xi_0^{(1)}$, ..., $\xi_0^{(12)}$. The surface-layer chains expanding in sideways from $C_{(0)}$ to $C_{(1)}$, $C_{(5)}$ and $C_{(9)}$ are designated as $s1$, $s2$ and $s3$ and the 13 inter-layer chains, which begin from the 13 surface-layer atoms, are numbered as 0, 1, 2, ..., 12. For example, the sequence of atomic vibrations for $s1$ is $\xi_0^{(0)}$, $\xi_0^{(1)}$, $\xi_0^{(2)}$, ..., which is equivalent to the notation $\xi_0^{(s1)}$, $\xi_1^{(s1)}$, $\xi_2^{(s1)}$, ... i.e., $\xi_0^{(0)} = \xi_0^{(s1)}$, $\xi_0^{(1)} = \xi_1^{(s1)}$ and $\xi_0^{(2)} = \xi_2^{(s1)}$. We note that the $s1$ sequence branches out from $\xi_0^{(0)}$ to $\xi_0^{(1)}$ and $\xi_0^{(12)}$, so the equivalent direction is $\xi_0^{(0)}$, $\xi_0^{(1)}$, $\xi_0^{(12)}$, ... Such branching continues as the sequence progresses, and in studying the propagation of energy from the reaction site to the bulk phase in the present paper, we select the sequence that represents the shortest distance between the site and the phase. The vibrational coordinates between inter-layers are similarly sequenced. For the 0th chain, the sequence is $\xi_0^{(0)}$, $\xi_0^{(1)}$, ..., $\xi_N^{(0)}$, where the N th atom is bound to the bulk phase. Similarly, each surface-layer chain consists of $N+1$ atoms. For $s1$, the vibrational sequence is $\xi_0^{(s1)}$, $\xi_1^{(s1)}$, ..., $\xi_N^{(s1)}$. The adsorption site $C_{(0)}$ is located at the center of the 13-atom arrangement and four chains (three sideways, one downward) originating from it. With the downward chains from the twelve adjacent atoms, we thus have 16 chains, identified by the superscripts $s1$, $s2$, $s3$, 0, 1, 2, ..., 12 in the vibrational coordinates. We find the chain length of 11 carbon atoms, i.e., $N = 10$, in both the surface layer and inter-layer directions is sufficient to account for the effects of surface atoms on the gas-atom interaction in the model. The choice of $N = 10$ is based on the preliminary result that energy transfer to the surface levels off to a constant value for $N > 5$.²² We take such a sufficiently large value of $N = 10$ to ensure that the chain length does not affect our results. The last member of each chain is the 11th carbon atom and it is bound to the bulk phase.

The distance between the successive inter-layers is 3.40 Å compared to the much shorter value of 1.42 Å for the C-C distance, d_{CC} , in the surface layer.⁴ Carbon atoms between adjacent layers in graphite are packed following two different arrangements. In one case an atom is directly above that of the next layer, whereas in the other an atom is above the hollow center of a hexagon of the next layer.²⁷⁻²⁹ Thus, for the multiple layers of C_{13} configuration, seven atoms couple to the atoms of the next layer via a straight chain, whereas the six atoms couple through a zigzag chain. Such

configurations are considered in the 13 inter-layer chain model. The 13 ($N+1$)-atom inter-layer chain model introduces a quasi-physical picture of energy flow between the reaction zone of $H(g)+H(ad)/C_{(0)}$ and the inter-layer atoms and, in turn, between the chain and the heat bath. This downward process and energy transfer to the surface-layer chains determine the role of the surface relaxation.

The details of the reaction-zone coordinates are shown in Figure 1b. A total of six degrees of freedom is required to describe the motions of $H(g)$ and $H(ad)$ above the adsorption site $C_{(0)}$. The coordinates for the adatom $H(ad)(x', y', z')$ with respect to the surface site $C_{(0)}$ are $x' = R_{CH}\sin\theta\cos\phi$, $y' = R_{CH}\sin\theta\sin\phi$, and $z' = R_{CH}\cos\theta + 0.35$ Å, where 0.35 Å represents $C_{(0)}$ puckering out of the surface plane, and the equilibrium bond distance $R_{CH,e}$ is 1.15 Å.⁴ In the model, we consider $C_{(0)}$ to remain in the puckered position during the reaction.¹⁷ Thus, the natural coordinate system for the $H(ad)-C_{(0)}$ oscillator is $H(ad)(R_{CH}, \theta, \phi)$. Previous studies show that it requires 0.89 eV to distort $C_{(0)}$ out of the substrate plane.^{17,18,30,31} Since the chemisorption well depth is 0.44 eV, the $H(ad)-C_{(0)}$ adsorption occurs with an energy of 1.33 eV at the equilibrium distance 1.50 Å. For the coordinates of the incident gas atom $H(g)(x, y, z)$, we note that the $H(g)$ -to- $H(ad)$ distance is $R_{HH} = (\rho^2 + z^2)^{1/2}$, where the initial ($t \rightarrow -\infty$) value of ρ is the impact parameter b . The projection of R_{HH} on the surface plane is oriented by the angle Φ from the X axis, and the vertical distance from $H(g)$ to the surface is $Z = z + R_{CH}\cos\theta + 0.35$ Å. Note that the X axis passes through $C_{(0)}$ and $C_{(1)}$, whereas the Y axis passes through $C_{(0)}$ and $C_{(4)}$. We set the origin of the XYZ coordinate system to be the unpuckered position $C_{(0)}$ in the basal plane. Thus, for $H(g)$, we use the cylindrical system (ρ, z, Φ) . The initial state of the reaction zone is $H(g)$ approaching the surface with the collision energy E , impact parameter b , and the azimuthal angle Φ from a large distance from the surface (15 Å), when $H(ad)$ is in the initial set of (R_{CH}, θ, ϕ) . The distance between $H(g)$ and $C_{(i)}$ is denoted by r_i , which has the functional dependence $r_i(R_{CH}, \theta, \phi, \rho, z, \Phi)$. In order to avoid the sketch becoming too crowded, we show only r_2 in Figure 1b.

We employ a potential energy surface (PES) constructed using a modified LEPS procedure.^{15,16} Although only three atoms are in the reaction zone, the incident atom is interacting with all 13 surface atoms, all of which have to be included in the PES. Furthermore, the interatomic vibrations of all chain atoms will also have to be included in the overall PES function which is a modified version of the LEPS procedure. We denote the overall function by $U(R_{CH}, \theta, \phi, \rho, z, \Phi, \{\xi\})$, where $\{\xi\}$ is the collective notation for all 16 chains each consisting of ($N+1$) vibrational coordinates, ξ_0 , ξ_1 , ξ_2 , ..., ξ_N as defined above. Thus the potential energy contains the effects of the vibrational motions of all chain atoms considered in the study. Each chain atom vibrates with the harmonic potential energy $\frac{1}{2}m_C\omega_{e_j}^2\xi_j^2$, and it couples with the adjacent atoms through $\frac{1}{2}m_C\omega_{c_j}^2\xi_{j-1}\xi_j$ and $\frac{1}{2}m_C\omega_{c_{j+1}}^2\xi_j\xi_{j+1}$, where m_C is the mass of the C atom, ω_{e_j} is the Einstein frequency and ω_{c_j} the coupling constant characterizing the chain. The $H(ad)-C_{(0)}$ bond undergoes

hindered motions along θ and ϕ , which can be treated as low-frequency harmonic vibrations about the Z axis. The overall PES function can then be given by

$$\begin{aligned}
 U(R_{\text{CH}}, \theta, \phi, \rho, z, \Phi, \{\xi\}) = & Q_{\text{HH}} + Q_{\text{HC}} + Q_{\text{HS}} \\
 & - [A_{\text{HH}}^2 + A_{\text{HC}}^2 + A_{\text{HS}}^2 - A_{\text{HH}}A_{\text{HC}} - (A_{\text{HH}} + A_{\text{HC}})A_{\text{HS}}]^{1/2} \\
 & + 1/2k_{\theta}\theta^2 + 1/2k_{\phi}\phi^2 + \sum_{s=1}^3 \sum_j [(1/2m_C\omega_{e,j}^2\xi_j^2)_s \\
 & + (\text{terms of type } \omega_{c,j}^2\xi_{j-1}\xi_j, \omega_{c,j+1}^2\xi_j\xi_{j+1}, \text{ etc})] \\
 & + \sum_{i=0}^{12} \sum_j [(1/2m_C\omega_{e,j}^2\xi_j^2)_i \\
 & + (\text{terms of type } \omega_{c,j}^2\xi_{j-1}\xi_j, \omega_{c,j+1}^2\xi_j\xi_{j+1}, \text{ etc})], \quad (1)
 \end{aligned}$$

where k_{θ} and k_{ϕ} are the force constants and the s -sum covers three surface-layer chains, whereas the i -sum is for 13 inter-layer chains, each chain consisting of 11 atoms. In Eq. (1) the subscript HH is for the H(g)-H(ad) interaction, HC for H(ad)-C₍₀₎ and HS for all H(g)-C_(i) including C₍₀₎. The coulombic and exchange terms for the H(g)-H(ad) are

$$\begin{aligned}
 Q_{\text{HH}} = & 1/4D_{\text{HH}}(1 + \Delta_{\text{HH}})^{-1}[(3 + \Delta_{\text{HH}})e^{(R_{\text{HH},e} - R_{\text{HH}})/a_{\text{HH}}} \\
 & - (2 + 6\Delta_{\text{HH}})e^{(R_{\text{HH},e} - R_{\text{HH}})/2a_{\text{HH}}}], \quad (2a)
 \end{aligned}$$

$$\begin{aligned}
 A_{\text{HH}} = & 1/4D_{\text{HH}}(1 + \Delta_{\text{HH}})^{-1}[(1 + 3\Delta_{\text{HH}})e^{(R_{\text{HH},e} - R_{\text{HH}})/a_{\text{HH}}} \\
 & - (6 + 2\Delta_{\text{HH}})e^{(R_{\text{HH},e} - R_{\text{HH}})/2a_{\text{HH}}}], \quad (2b)
 \end{aligned}$$

and the similar expressions for H(ad)-C₍₀₎, where D and a are the potential parameters and $R_{\text{HH},e}$ is the equilibrium distance of the HH bond. In Eq. (1), Q_{HS} and A_{HS} stand for the interaction of H(g) with the 13 surface atoms. The coulombic and exchange energies for the HS interaction include many H(g)-C_(i) terms thus modifying the LEPS part of the PES significantly as shown below:

$$\begin{aligned}
 Q_{\text{HS}} = & 1/4D_{\text{HS}}(1 + \Delta_{\text{HS}})^{-1} \sum_{j=0}^{12} [(3 + \Delta_{\text{HS}})e^{(R_{\text{HS},e} - R_{\text{HS}})/a_{\text{HS}}} \\
 & - (2 + 6\Delta_{\text{HS}})e^{(R_{\text{HS},e} - R_{\text{HS}})/2a_{\text{HS}}}]_i, \quad (2c)
 \end{aligned}$$

$$\begin{aligned}
 A_{\text{HS}} = & 1/4D_{\text{HS}}(1 + \Delta_{\text{HS}})^{-1} \sum_{j=0}^{12} [(1 + 3\Delta_{\text{HS}})e^{(R_{\text{HS},e} - R_{\text{HS}})/a_{\text{HS}}} \\
 & - (6 + 2\Delta_{\text{HS}})e^{(R_{\text{HS},e} - R_{\text{HS}})/2a_{\text{HS}}}]_i. \quad (2d)
 \end{aligned}$$

Each coulombic or exchange term of the LEPS function contains the Sato parameter (Δ). For the H(g)-H(ad) interaction, we use the binding energy of H₂ in its ground state $D_0^0 = 4.4781$ eV at $R_{\text{HH},e} = 0.7414$ Å.³² With the frequency $\omega_{\text{HH}}/2\pi c = 4401$ cm⁻¹,³² we find the exponential range parameter $a_{\text{HH}} = (D_{\text{HH}}/2\mu_{\text{HH}})^{1/2}/\omega_{\text{HH}} = 0.257$ Å, where $D_{\text{HH}} = D_0^0 + 1/2 \hbar \omega_{\text{HH}}$. For H(ad) chemisorbed on a graphite surface, *i.e.*, the H(ad)-C₍₀₎ bond, we take the binding energy of $D_{\text{HC}} = 1.33$ eV, as noted above. As the nascent H-H bond forms, the initially puckered C₍₀₎ breaks its bond with H(ad) and relaxes back to its surface lattice position, thus releasing 0.89 eV, so the exoergicity of the reaction is $4.4781 - 0.44 = 4.04$ eV. Thus, H₂(g) can be formed in its first 12 vibrational states at zero collision energy.¹⁸ We use the observed H(ad)-

C₍₀₎ stretching and H(ad)-C₍₀₎-C₍₁₎ bending frequencies of $H_{\text{C,st}} = 2710$ cm⁻¹ and $H_{\text{C,bend}} = 1250$ cm⁻¹, respectively.³³ The exponential range parameter is then $a_{\text{HC}} = (D_{\text{HC}}/2\mu_{\text{HC}})^{1/2}/\omega_{\text{HC,st}} = 0.166$ Å. For the H(g)-surface interaction, the physisorption energy D_{HS} is 0.043 eV and $a_{\text{HS}} = 0.368$ Å.^{13,19} In addition to this physisorption-type interaction, we also consider H(g) interacting with the unpuckered surface atoms with a stronger interaction of the chemisorption type.

Within the framework of density functional theory, Morisset *et al.* have shown a low barrier of 9.2 meV when the zero-point energy of the degrees of freedom perpendicular to the minimum energy path is taken into account.¹⁸ From extensive preliminary calculations, we find no product molecules being trapped in the exit valley. Furthermore, the probability of the incident atom trapped in the entrance valley without recombination is found to be in the order of 10⁻⁴, which indicates the absence or near-absence of a shallow attractive well in the valley. By varying the Sato parameters systematically for the interaction energies (D 's) and equilibrium distances given above, we obtained the parameters which best describe the desired features of a low energy barrier height 9.2 meV and no attractive well in both the entrance and exist channel to be $\Delta_{\text{HH}} = 0.15$, $\Delta_{\text{HC}(0)} = 0.80$, $\Delta_{\text{HS}} = 0.20$ for H(g)-C₍₀₎ and $\Delta_{\text{HS}} = 0.11$ for H(g)-C_(i), $i = 1-12$. For the H(g)-surface physisorption interaction, these delta values yield the HS equilibrium distance of 3.46 Å, which is fairly close to 3.6 Å reported in ref. 17.

The attractive PES constructed using these parameters in Eq. (1) is shown in Figure 2a in the direction $\theta = \phi = \Phi = 0^\circ$ for $b = 0$. We have found that the PES for the chosen deltas remain essentially unchanged when the angles are displaced by 10° or the impact parameter by 0.5 Å. An enlarged contour plot near the short range between H(ad)-C₍₀₎ and H(g)-H(ad) is shown in Figure 2b, where the chosen deltas and the equilibrium H-surface distance are used in the potential function to obtain the barrier of $|-1.3208$ eV - (-1.33 eV) = 9.2 meV in the entrance valley, the value reported by Morisset *et al.*¹⁸ An important aspect of the PES constructed in the present study is the existence of such a barrier, even though it is low, which can significantly affect the H₂ recombination at the low collision energies of an extreme temperature environment (*e.g.*, interstellar medium). We have checked the region between the H-H distances 2.8 and 3.3 Å along the minimum energy path on an enlarged scale and found that the energy profile is essentially identical to that shown by Morisset *et al.* Figure 2c shows the minimum energy path along the reaction coordinate; the inset shows the barrier height of 9.2 meV. The position of the barrier clearly indicates the topology of an early downhill surface in the entrance valley, which can lead to an early release of the reaction energy and high vibrational excitation. The PES depends on two coordinates, the H(ad)-C₍₀₎ and H(g)-H(ad) bonds, the former being broken and the latter formed in the recombination reaction. Inclusion of the many-body effects coming from the surface atoms in the construction of potential energy surfaces for gas-surface reactions is very difficult, but the present approach provides a sufficiently

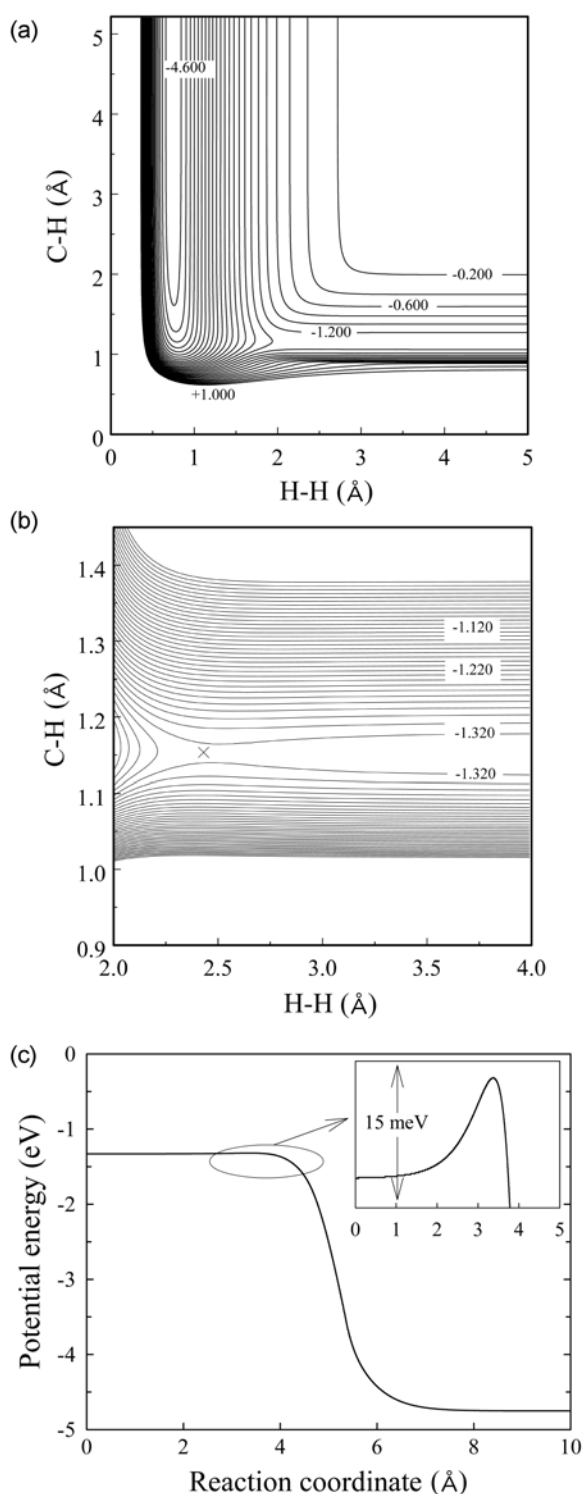


Figure 2. Attractive potential energy surfaces. The coordinates are the H(g)-H(ad) distance in the entrance valley and C₍₀₎-H(ad) in the exit valley. (a) The entire potential region is shown in the direction of $\theta = \phi = \Phi = 0^\circ$ for the $b = 0$ collision. The minimum of the exit valley is $D_{\text{HH}} = 4.70$ eV. The labeled contours are in eV. (b) The barrier region and the entrance channel are enlarged. A barrier occurs at the energy -1.3208 eV, indicated by a cross. (c) Minimum energy path. The barrier region is enlarged in the inset.

detailed PES capable of elucidating the problems stated in the present study.

To study the reaction dynamics, we follow the time evolution of the reaction system by integrating the equations of motion, which describe the motions of H(g), H(ad), and all atoms of 16 carbon chains. The equations of motion of the six coordinates describing the incident and chemisorbed hydrogen atoms are

$$m_{\text{H}}\ddot{Z}(t) = -U(R_{\text{CH}}, \theta, \phi, \rho, z, \Phi, \{\xi\})/Z, \quad (3a)$$

$$\mu_{\text{HH}}\ddot{\rho}(t) = -U(R_{\text{CH}}, \theta, \phi, \rho, z, \Phi, \{\xi\})/\rho, \quad (3b)$$

$$I_{\text{HH}}\ddot{\Phi}(t) = -U(R_{\text{CH}}, \theta, \phi, \rho, z, \Phi, \{\xi\})/\Phi, \quad (3c)$$

$$\mu_{\text{CH}}\ddot{R}_{\text{CH}}(t) = -U(R_{\text{CH}}, \theta, \phi, \rho, z, \Phi, \{\xi\})/R_{\text{CH}}, \quad (3d)$$

$$I_{\text{CH}}\ddot{\theta}(t) = -U(R_{\text{CH}}, \theta, \phi, \rho, z, \Phi, \{\xi\})/\theta, \quad (3e)$$

$$I_{\text{CH}}\ddot{\phi}(t) = -U(R_{\text{CH}}, \theta, \phi, \rho, z, \Phi, \{\xi\})/\phi, \quad (3f)$$

where m_{H} is the mass of H, μ_{HH} is the reduced mass of H₂, μ_{CH} is the reduced mass of CH, I_{HH} is the moment of inertia of H₂ and I_{CH} is the moment of inertia of CH. For each of (N+1)-atom surface-layer and inter-layer chains, the equations of motion are¹⁶

$$m_{\text{C}}\ddot{\xi}_0(t) = -m_{\text{C}}\omega_{e,0}^2\xi_0(t) + m_{\text{C}}\omega_{e,1}^2\xi_1(t) - U(R_{\text{CH}}, \theta, \phi, \rho, z, \Phi, \{\xi\})/\xi_0, \quad (4a)$$

$$m_{\text{C}}\ddot{\xi}_1(t) = -m_{\text{C}}\omega_{e,1}^2\xi_1(t) + m_{\text{C}}\omega_{e,0}^2\xi_0(t) + m_{\text{C}}\omega_{e,2}^2\xi_2(t), \quad (4b)$$

$$m_{\text{C}}\ddot{\xi}_j(t) = -m_{\text{C}}\omega_{e,j}^2\xi_j(t) + m_{\text{C}}\omega_{e,j-1}^2\xi_{j-1}(t) + m_{\text{C}}\omega_{e,j+1}^2\xi_{j+1}(t), \quad j = 2, \dots, N-1 \quad (4c)$$

$$m_{\text{C}}\ddot{\xi}_N(t) = -m_{\text{C}}\Omega_N^2\xi_N(t) + m_{\text{C}}\omega_{e,N}^2\xi_{N-1}(t) - m_{\text{C}}\beta_{N+1}\dot{\xi}_N(t) + m_{\text{C}}f_{N+1}(t). \quad (4d)$$

In the above equations, Ω_N is the adiabatic frequency which determines the long-time response of the heat bath, β_{N+1} is the friction coefficient governing the dissipation of energy from the reaction zone, and $f_{N+1}(t)$ determines the random force on the reaction zone arising from thermal fluctuation in the heat bath.³⁴ The friction coefficient is very close to $\omega_{\text{D}}/6$, where ω_{D} is the Debye frequency 420 K for graphite.³⁵ All values of the frequencies and friction coefficients in Eqs. (4a-4d) are presented elsewhere.²² Note that in Eq. (4d) the random force term balances, on average, the dissipative force $m_{\text{C}}\beta_{N+1}\dot{\xi}_N(t)$, which removes energy from the reaction zone in order that the equilibrium distribution of energies in the reaction zone be restored after collision. We can carry out the rigorous dynamical calculation of the present gas-surface reaction system with the above set of equations of motion based on the PES constructed above.

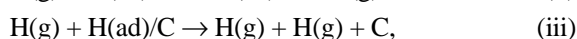
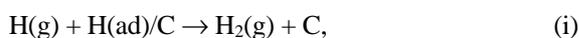
The initial conditions for the equations of motion are given in an earlier paper.³⁶ The numerical procedures include the use of Monte Carlo routines to generate random numbers for the initial conditions. We sample collision energies E from a Maxwell distribution at gas temperature T_{g} and weigh the initial energy of H(ad)-C₍₀₎ and chain atom vibrations by a Boltzmann distribution at surface temperature T_{s} . The normal component of the incident energy is $E\cos^2\theta_{\text{inc}}$, where $\theta_{\text{inc}} = \arctan(\rho/z)$ is the incident angle defined in Figure 1. In sampling impact parameters b , we take the flat range of $0 < b < b_{\text{max}}$, where b_{max} is taken to be $2d_{\text{CC}}$. This value is the

distance between the unpuckered position of $C_{(0)}$ in the XY plane and the farthest sites $C_{(3)}$, $C_{(7)}$ and $C_{(11)}$ in the model. Such a wide range of b from the adatom site will enable us to treat all important trajectories, capable of producing the H(ad)- $C_{(0)}$ dissociation and H_2 formation. Also sampled are the initial values θ_0 , ϕ_0 , and Φ_0 . Thus each trajectory is generated with the set $(E, b, E_{CH}^0, \theta_0, \phi_0, \Phi_0, \{\xi\}_0)$, where E_{CH}^0 is the initial vibrational energy of the H(ad)- $C_{(0)}$ bond. The total number of trajectories sampled for each run is 40,000.

In studying the time evolution of the recombination reaction, we follow each trajectory for 50 ps, which is sufficiently long time for $H_2(g)$ to recede from the influence of surface interaction, to confirm the occurrence of a reactive event. For the recombination reaction, we define the reaction time t_R as the duration between the first instance at which the incident atom reaches the closest distance to H(ad), *i.e.*, the first turning point, and the time at which the dissociating H(ad) reaches 5 Å, where H(g)-H(ad) stabilizes to $H_2(g)$. Furthermore, we confirm that each trajectory can be successfully back-integrated in the numerical procedure.

Results and Discussion

In the present gas surface collision system, we find the following reaction pathways:



Reaction (i), the recombination reaction, is the main subject of our study in the present paper. In the H-H exchange reaction represented by Reaction (ii), the adatom desorbs as the incident atom adsorbs on the adatom site $C_{(0)}$ or one of the nearby sites $C_{(i)}$ as H(ad) desorbs. The collision induced dissociation of H(ad) is shown by Reaction (iii), where both hydrogen atoms are in the gas phase without recombining. Reaction (iv) is the adsorption of the incident atom on one of the empty sites $C_{(i)}$.

The H(g)-surface interaction can be either the physisorption type or chemisorption type. The incident atom feels only a weak physisorption-type interaction with the bare surface atom. However, at high collision energies, the chemisorption-type interaction can become important. We thus consider both types in the calculation. On the same potential energy surface, we first perform the calculation for the physisorption-type interaction. We then combine to this result, the reactive trajectories found in the chemisorption-type interaction excluding those trajectories which have already found to be reactive in the physisorption calculation. All four reactive probabilities will be calculated using the total reactive trajectories determined in this manner. For each interaction type, the reaction probability is defined as the ratio of the number of reactive trajectories to the total number of trajectories sampled. In the recombination

reaction, the expressions needed to determine the amounts of energy carried by $H_2(g)$ in the form of vibration, rotation and translation are, respectively,

$$E_{v,HH} = \frac{1}{2}\mu_{HH}\dot{R}_{HH}^2 + D_{HH}[1 - e^{(R_{HH,e} - R_{HH})/a_{HH}}]^2, \quad (5a)$$

$$E_{r,HH} = L_{HH}^2/2\mu_{HH}R_{HH}^2, \quad (5b)$$

$$E_{t,HH} = \frac{1}{2}m_{HH}(\dot{Z} - \frac{1}{2}\dot{R}_{HH}\cos\theta_{inc})^2, \quad (5c)$$

where L_{HH} is the angular momentum $\mu_{HH}(z\dot{\rho} - \dot{z}\rho)$ corresponding to the quantum number $J_{HH} = L_{HH}/\hbar$ and m_{HH} is the mass of H_2 . The expression for the energy propagated from the reaction zone to the solid phase through the $(N+1)$ -atom chains for the collision leading to the H_2 formation is

$$\begin{aligned} E_{s,HH} = & \sum_{s=1}^3 [\frac{1}{2}m_C \sum_{j=0}^N \xi_j^2(t) + \frac{1}{2}m_C \sum_{j=0}^{N-1} \omega_{e,j}^2 \xi_j^2(t) \\ & + \frac{1}{2}m_C \Omega_N^2 \xi_N^2(t) + m_C \sum_{j=0}^{N-1} \omega_{e,j+1}^2 \xi_j(t) \xi_{j+1}(t)]_s \\ & + \sum_{i=1}^{12} [\frac{1}{2}m_C \sum_{j=0}^N \xi_j^2(t) + \frac{1}{2}m_C \sum_{j=0}^{N-1} \omega_{e,j}^2 \xi_j^2(t) \\ & + \frac{1}{2}m_C \Omega_N^2 \xi_N^2(t) + m_C \sum_{j=0}^{N-1} \omega_{e,j+1}^2 \xi_j(t) \xi_{j+1}(t)]_i. \quad (6) \end{aligned}$$

We average each of these energies over the ensemble of reactive trajectories forming H_2 to obtain the quantities $\langle E_{v,HH} \rangle$, $\langle E_{r,HH} \rangle$, $\langle E_{t,HH} \rangle$ and $\langle E_{s,HH} \rangle$, which include the contributions from both physisorption and chemisorption-type H(g)-surface interaction. Note that although it is not an energy transfer step to H_2 , we use the subscript HH in $\langle E_{s,HH} \rangle$ to represent its association with the H_2 recombination pathway. We now discuss the results of reaction probability and energy transfer calculations obtained for two different temperature sets, $(T_g, T_s) = (1500 \text{ K}, 300 \text{ K})$ and $(10-100 \text{ K}, 10 \text{ K})$.

A. Reactions at High Temperatures. The probabilities of Reactions (i)-(iv) for the collisions taking place at $T_g = 1500 \text{ K}$ and $T_s = 300 \text{ K}$ are $P_{(i)} = 0.284$, $P_{(ii)} = 0.011$, $P_{(iii)} = 0.239$ and $P_{(iv)} = 0.005$, respectively. The chosen gas temperature is near the lower end of the filament temperature used in experimental studies.³⁷ Thus the temperature condition mimics H(g) produced in a tungsten filament chamber interacting with a graphite surface, which is maintained at room temperature. The reactive event takes place on a subpicosecond time scale. As shown in Figure 3, the majority of reactive events occur at a reaction time t_R below 0.1 ps with the maximum value of the reaction probability occurring near 20 fs. Here the plot is prepared by summing reactive trajectories in a given time interval and dividing the sum by the total number of trajectories sampled; *e.g.*, the number of reactive trajectories between $t = 25.0$ fs and 50.0 fs is 3056 and, therefore, the corresponding probability is 3056/40,000 = 0.0764, which is plotted at the midpoint 37.5 fs.

In Figure 4a, we present the time evolution of the distances of H(g)-surface, H(ad)- $C_{(0)}$ and H(g)-H(ad) for a trajectory representing the recombination event. The incident atom approaches the closest distance near $t = 0$. We can

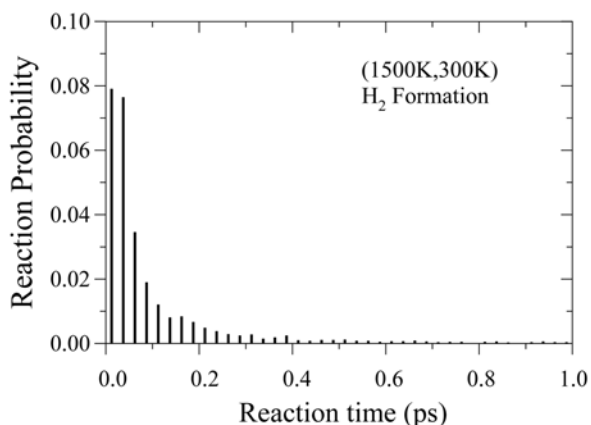


Figure 3. The distribution of reaction times of the $\text{H}_2(\text{g})$ formation at (1500 K, 300 K).

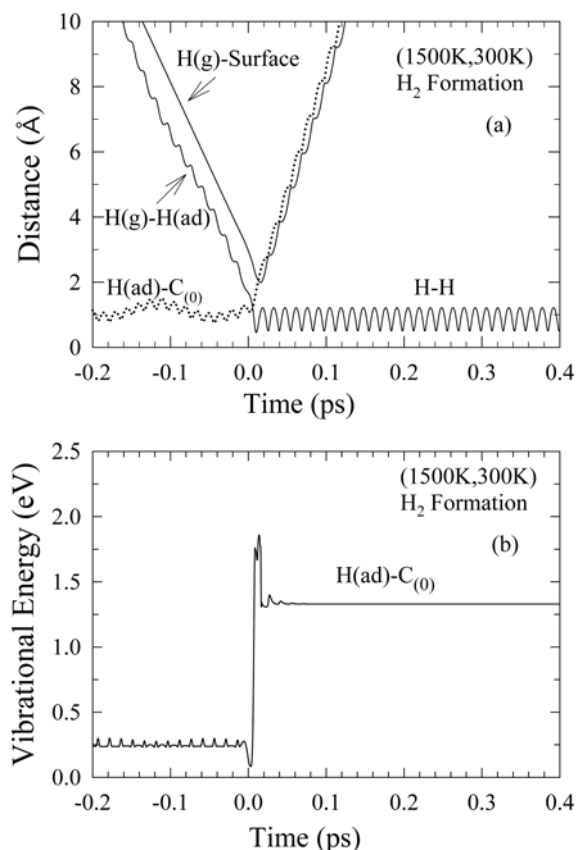


Figure 4. Dynamics of a representative trajectory for the recombination reaction at (1500 K, 300 K). (a) Time evolution of collision and bond trajectories. (b) Time evolution of the vibrational energy of the dissociating $\text{H}(\text{ad})\text{-C}_{(0)}$ bond.

identify the $\text{H}(\text{g})\text{-surface}$ distance as the collision trajectory. Before and after reaching the turning point, a significant amount of acceleration of the collision trajectory occurs, the process which leads to energy transfer to the $\text{H}(\text{ad})\text{-C}_{(0)}$ vibration. As seen in Figure 4a, the $\text{H}(\text{ad})\text{-C}_{(0)}$ distance rises rapidly as the collision trajectory turns the corner indicating that the dissociating atom is attracted to the incident atom before it rebounds, thus forming the nascent H-H bond which then recedes rapidly from the surface.

The time evolution of the $\text{H}(\text{g})\text{-surface}$, $\text{H}(\text{g})\text{-H}(\text{ad})$ and $\text{H}(\text{ad})\text{-C}_{(0)}$ distances in the neighborhood of $t=0$ reveals detailed aspects of the dynamics of the recombination. At the initial impact, $\text{H}(\text{g})$ reaches $\text{H}(\text{ad})$ within a distance of 0.45 \AA , which is far shorter than the equilibrium H-H bond distance 0.74 \AA . The $\text{H}(\text{g})\text{-H}(\text{ad})$ distance then bounces back to 1.22 \AA before the atoms are attracted back to each other for the separation of 0.50 \AA . After the oscillation, the vibrational motion of the nascent $\text{H}(\text{g})\text{-H}(\text{ad})$ bond is stabilized to form H_2 , which oscillates between the upper and lower limits. In Figure 4a such highly regular vibration is clearly seen and it immediately follows the initial impact between $\text{H}(\text{g})$ and $\text{H}(\text{ad})$. The time evolution of the H-H distance corresponds to the bond oscillating at a frequency of 2270 cm^{-1} , which represents a highly excited state. It should be noted that the outgoing portion of the $\text{H}(\text{g})\text{-surface}$ distance shown in Figure 4a no longer represents the collision trajectory. It describes the time evolution of the diverging distance between $\text{H}(\text{g})$ of $\text{H}_2(\text{g})$ and the surface. Similarly, the post-turning-point portion of the $\text{H}(\text{ad})\text{-C}_{(0)}$ distance is not the bond trajectory of $\text{H}(\text{ad})\text{-C}_{(0)}$ but the distance between $\text{H}(\text{ad})$ of $\text{H}_2(\text{g})$ and $\text{C}_{(0)}$. The time evolution of these distances suggests that the $\text{H}(\text{ad})\text{-C}_{(0)}$ dissociation and $\text{H}(\text{g})\text{-H}(\text{ad})$ recombination processes in the representative trajectory occur in a brief period of slightly over 30 fs, after which the excited product oscillates with the period of 15 fs. Note that the vibrational period of the ground-state $\text{H}(\text{ad})\text{-C}_{(0)}$ bond is 12 fs and that of the ground-state H-H bond is 7.6 fs. Their oscillatory variations of the $\text{H}(\text{g})\text{-surface}$ and $\text{H}(\text{ad})\text{-C}_{(0)}$ curves in the post-collision region shown in Figure 4a are particularly illustrative as they describe the vibrational motion of the outgoing $\text{H}_2(\text{g})$. In Figure 4b, we plot the time evolution of the $\text{H}(\text{ad})\text{-C}_{(0)}$ vibrational energy. The vibrational energy rises sharply near the instance of the initial impact of $\text{H}(\text{g})$ on $\text{H}(\text{ad})$. The $\text{H}(\text{ad})\text{-C}_{(0)}$ bond gains nearly 1.6 eV from the incident atom in a strong collision and then retains most of it to disrupt the bond, which occurs near the end of the initial vibration of the nascent H-H bond shown in Figure 4a. Beyond the period of about 30 fs after the $\text{H}(\text{g})\text{-H}(\text{ad})$ impact, the curve levels off to a value slightly higher than the bond energy 1.33 eV. The constant value of the vibrational energy beyond $t=40$ fs simply implies that the $\text{H}(\text{ad})\text{-C}_{(0)}$ bond dissociation has occurred. The curves shown in both Figures 4a and 4b clearly indicate the direct-mode mechanism of $\text{H}(\text{g})\text{-H}(\text{ad})$ recombination taking place on a subpicosecond time scale. It should be noted that the time scale shown in Figure 4 is the result of the numerical framework we used in solving the equations of motion, so what is important in analyzing the time evolution is time intervals rather than absolute values.

The opacity function, which is the reaction probability expressed as a function of impact parameter b , shown in Figure 5 takes values around 0.4 as b increases from zero taking the maximum value of ≈ 0.7 near $b=0.6 \text{ \AA}$. It should be noted that b is the initial value of ρ , which evolves in time according to Eq. (3b). The function is calculated by summing the number of recombination trajectories and dividing it

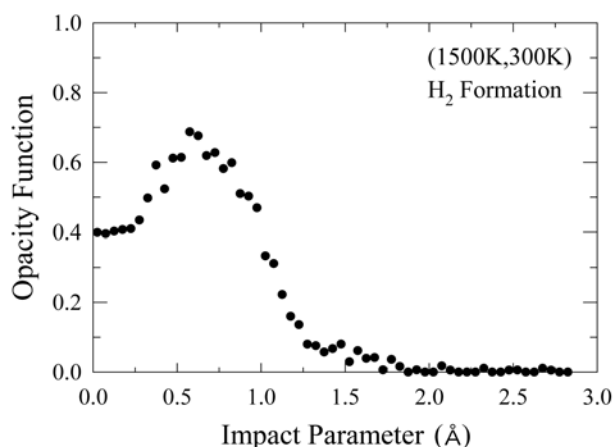


Figure 5. The dependence of the opacity function of $\text{H}_2(\text{g})$ formation on the impact parameter at (1500 K, 300 K).

by the total number of trajectories in a given b interval. For example, between $b = 0.10 \text{ \AA}$ and 0.15 \AA , the number of reactive trajectories is 248 and the total number of trajectories is 616, so the opacity function is $248/616 = 0.403$, which is plotted at the midpoint 0.125 \AA in Figure 5. Beyond the impact parameter 1.0 \AA , the opacity function decreases sharply. For example, at $b = 2.0 \text{ \AA}$ it is only 0.01, suggesting that the effects of the second and third nearest surface atoms are unimportant in the recombination. The result indicates that the $\text{H}(\text{g})\text{-H}(\text{ad})$ collision with b in the neighborhood of $R_{\text{HH},e} = 0.7414 \text{ \AA}$ occurring in such a short subpicosecond time scale is particularly efficient for the recombination. Also efficient are head-on or near head-on collisions. Although it is a different system, it is interesting to note that such structured b -dependence of the opacity function has been known in a direct reaction between $\text{H}(\text{g})$ and $\text{H}(\text{ad})$ on a copper surface³⁸ and on a tungsten surface.³⁹

The ensemble-averaged collision energy of all reactive trajectories at (1500 K, 300 K) is 0.652 eV, which is in the high energy tail of the Maxwell distribution and exceeds the barrier to chemisorption. That is, most of the H_2 formation occurs at collision energies higher than $3/2 kT = 0.194 \text{ eV}$. In fact, we find nearly 60% of the recombination event, Reaction (i), occurs in the strong chemisorption-type $\text{H}(\text{g})\text{-surface}$ interaction. The rest is from the physisorption-type interaction.

For the entire reactive trajectories, $\langle E_{v,\text{HH}} \rangle$ is 2.01 eV, which is half the energy released by the recombination reaction (4.04 eV). Such efficient channeling of the reaction energy into product vibrational excitation is in accord with the expectations of an early release of the energy on the attractive PES shown in Figure 2. The trajectory slides down with an ample translational energy from the entrance valley but tends to continue in a straight line hitting the outer wall of the exit valley. The trajectory then bounces back and forth between the inner and outer wall thus causing the trajectory to deviate from the minimum energy path, which leads the $\text{H}(\text{g})\cdots(\text{ad})$ repulsion to convert the exoergicity into the product vibration.³⁸⁻⁴⁰ Thus the energetics of the present recombination reaction resembles those of $\text{F} + \text{H}_2 \rightarrow \text{H} + \text{HF}$,⁴⁰

$\text{K} + \text{Br}_2 \rightarrow \text{K}^+ + \text{Br}_2^-$,⁴¹ and $\text{O} + \text{H}/\text{Si} \rightarrow \text{OH} + \text{Si}$.¹⁵ Accumulation of such a large amount of energy in the vibration clearly suggests the occurrence of strong vibrational excitation of the product molecule in the gas-surface reaction. The remaining energy is distributed among the rotational and translational motions of H_2 and the surface; the amounts deposited in these motions are 9%, 33% and 8% of the reaction energy, respectively. It is interesting to note that the amount of energy shared by translation is large and it is far larger than the rotational energy. Although not large, energy transfer to the bulk solid phase is significant and it should be included in studying the energy disposal.

An interesting aspect of the energetics of H_2 formation is that for $\text{H}(\text{g})$ interacting with the surface through the physisorption-type force, the amounts of ensemble-averaged energies deposited in the vibration, rotation, translation and the bulk surface are 63, 9, 14, and 13% of the reaction energy, respectively, whereas for $\text{H}(\text{g})$ interacting with the surface through the chemisorption-type force, the corresponding values are 41, 9, 45, and 5%. That is, the vibrational motion is the major energy reservoir in the physisorption-type interaction, while translation shares most energy in the stronger chemisorption-type interaction. Energy transfer to the surface is significant in the former type. In both interactions, rotation plays a less important role in receiving the liberated energy.

To present a clearer picture of the vibrational excitation, we extract quantum analog of the classical calculation using a binning procedure of assigning vibrational quantum number ν corresponding to the calculated H_2 vibrational $\langle E_{v,\text{HH}} \rangle$ in the present study through the equation $\nu = \text{int}[\langle E_{v,\text{HH}} \rangle / E(\nu)]$, where “int” signifies the nearest integer including zero. In this procedure, we introduce the eigenvalue expression $E(\nu)$ calculated by Kolos, Szalewicz and Monkhorst (KSM) using the Born-Oppenheimer procedure for the electronic ground state of the hydrogen molecule.⁴² The KSM values vary from $G(\nu + 1/2) = 4161.166 \text{ cm}^{-1}$ for $\nu = 0$ to 621.794 cm^{-1} for $\nu = 13$. Experimental studies show that the 1413 transition frequency for the non-rotating H_2 is very close to 620 cm^{-1} .⁴³

In Figure 6, we show the vibrational population distribution of two types of the $\text{H}(\text{g})\text{-surface}$ interaction, that is, the physisorption-type and chemisorption-type. The sum of these two types is the total relative intensity and it is identified as “Total” in the plot. As noted above, in the total probability the physisorption-type and chemisorption-type contributions are 38 and 62%, respectively. For the low-lying levels ($\nu = 1\text{-}2$), the intensity of the chemisorption-type is higher than that of the physisorption-type e.g., for $\nu = 0$, the former is five times the latter. However, the situation is reversed from $\nu = 5$. A particularly noteworthy result seen in Figure 6 is that the vibrational population distribution of H_2 formed in the weak physisorption-type interaction is strongly inverted with the maximum appearing at $\nu = 3$. Because of a significant contribution to the recombination from the chemisorption-type interaction, the total intensity shows no inversion, although it does not follow the Boltzmann distri-

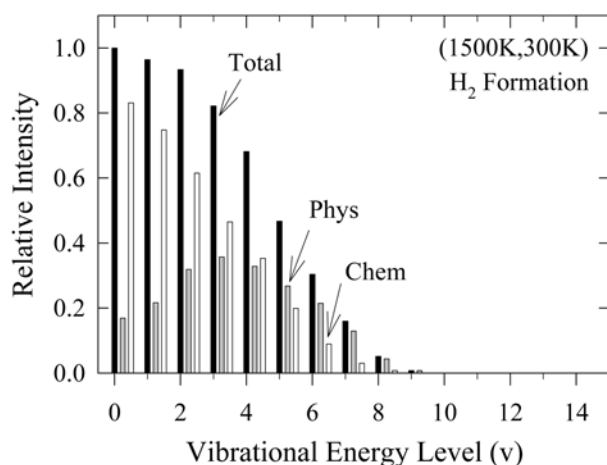


Figure 6. Vibrational population distribution of $\text{H}_2(\text{g})$ at (1500 K, 300 K). The shaded and open bars are for the physisorption and chemisorption-type interactions, respectively. The solid bar is for the total probability.

bution.

Before closing this section, we note that in reaction (iii), the collision-induced desorption pathway, the energetic incident atom has strong tendency to dislodge the adatom from the $\text{C}_{(0)}$ site in head-on or near head-on collisions, which are found to occur on a subpicosecond time scale. As in reaction (i), $\text{H}(\text{g})$ interacts to desorb $\text{H}(\text{ad})$ from the chemisorption site but it does not recombine with the desorbing atom in this reaction. In such an event, the desorbing atom from the chemisorption-type interaction recedes from the surface with a large amount of kinetic energy, thus making its capture by $\text{H}(\text{g})$ difficult. About 65% of the desorption reaction events, $P_{(\text{iii})} = 0.230$ as noted above, comes from the physisorption-type interaction.

B. Reactions at Low Temperatures. To study the gas-surface interaction at low temperatures, which mimic the interstellar environment,^{11,14,16,26,44-46} we first take the temperature condition, $(T_g, T_s) = (100 \text{ K}, 10 \text{ K})$ and consider the physisorption-type interaction to be operating. Note that at $T_g = 100 \text{ K}$, $kT = 8.6 \text{ meV}$, which is lower than the barrier height determined above. The reaction probabilities are found to be $P_{(\text{i})} = 0.059$, $P_{(\text{ii})} = 0.002$, $P_{(\text{iii})} = 0.090$ and $P_{(\text{iv})} = 0.006$, *i.e.*, the reaction is dominated by the collision-induced desorption process. As shown in Figure 7, the distribution of reaction times at (100 K, 10 K) is very different from that of the (1500 K, 300 K) system considered above in Figure 3. The time scale of H_2 formation is now significantly longer than that at (1500 K, 300 K) and the H_2 recombination does not occur before 0.07 ps, *i.e.*, unlike the (1500 K, 300 K) system, the low-temperature reaction occurs after a brief induction period. At the low temperature environment, where the $\text{H}(\text{g})$ -surface interaction is weak, the reaction requires a longer time for energy flow and the nascent $\text{H}(\text{g})\cdots\text{H}(\text{ad})$ bond to stabilize compared to the reaction at (1500 K, 300 K). As shown in Figure 7, the recombination events occur over a wide time range, taking the maximum probability near 0.2 ps. The extent of reaction with a reaction time as

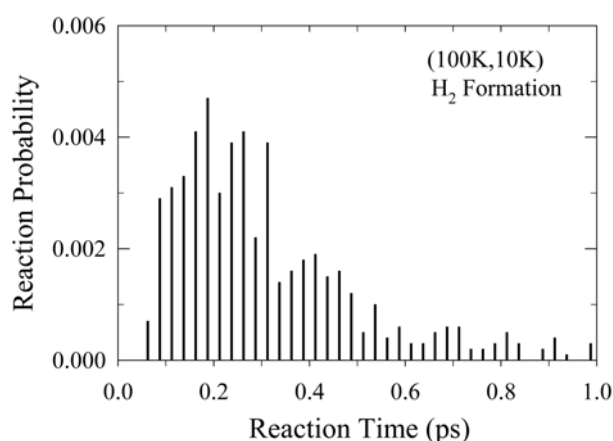


Figure 7. The distribution of reaction times of the $\text{H}_2(\text{g})$ formation at (100 K, 10 K).

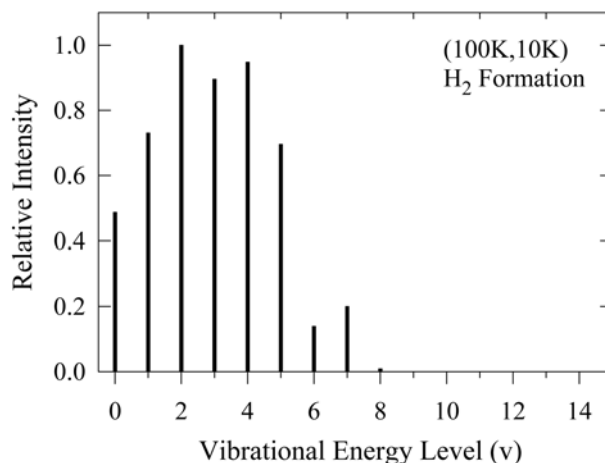


Figure 8. Vibrational population distribution of $\text{H}_2(\text{g})$ at (100 K, 10 K).

long as 0.8 ps is not negligible.

At (100 K, 10 K), 66% of the energy liberated by the recombination reaction is carried away by the vibrational motion of H_2 . This value is much larger than the (1500 K, 300 K) case, where it is 50%. However, a more important result is that translation shares only 16% of the released energy, which is far less than that of the high-temperature case. The amount of energy deposited in the rotation of H_2 and that propagated into the solid phase are 14% and 4%, respectively. The latter extent suggests that the surface relaxation process is inefficient at such a low temperature environment. As shown in Figure 8, the energy deposited in the vibrational motion leads to a significant population inversion as in the physisorption-type interaction case at (1500 K, 300 K) displayed in Figure 6. We find nearly all trajectories for the recombination reaction come from the incident atom, which approaches $\text{H}(\text{ad})$ from top with $\theta_{\text{inc}} < 90^\circ$, indicating that the slowly moving $\text{H}(\text{g})$ is attracted to $\text{H}(\text{ad})$ before it had a chance to come to close proximity of the surface.^{47,48} These recombination events occur in head-on or near head-on collisions as shown in Figure 9, where the opacity function is confined to the impact parameter range of 0 to $\approx 1.0 \text{ \AA}$, the distance which is less than the bond

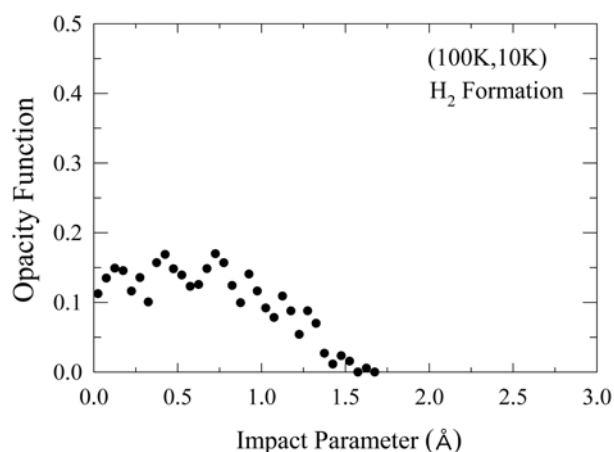


Figure 9. The dependence of the opacity function of $\text{H}_2(\text{g})$ formation on the impact parameter at (100 K, 10 K).

distance d_{CC} .

At (10 K, 10 K) the probabilities of all these reactions are in the order of 10^{-4} . The recombination probability is 0.05, 0.04, 0.02 and 0.004 at $T_g = 80, 60, 40$ and 20 K, respectively. As T_g is lowered from 100 K to 10 K, the exchange probability decreases from 0.0016 to 10^{-4} , whereas the adsorption probability varies from 0.006 to 10^{-4} . We note that even in the (1500 K, 300 K) condition considered in Sec. III-A, where the chemisorption-type interaction is found to be important, the exchange and adsorption probabilities are small compared to the two other probabilities; *i.e.*, $P_{(\text{ii})} = 0.011$ and $P_{(\text{iv})} = 0.0045$, indicating a near independence of the $\text{H}(\text{g})\text{-H}(\text{ad})$ exchange and $\text{H}(\text{g})$ adsorption processes on the gas and surface temperatures. As in (1500 K, 300 K), the desorption probability is significant. In fact, it is the largest in the temperature range, varying from 0.09 at $T_g = 100$ K to 0.05 at 50 K and then to 10^{-4} . Thus, although its magnitudes is not large, the latter probability, as well as the recombination probability, rises steadily with T_g at the extreme condition of $T_s = 10$ K. In closing this section, at the risk of repetition, it is worth mentioning that the values of $P_{(\text{i})} = 0.059$ and $P_{(\text{iii})} = 0.090$ at (100 K, 10 K) and $P_{(\text{i})} = 0.284$ and $P_{(\text{iv})} = 0.239$ at (1500 K, 300 K) are obtained in a 3-dimensional model, where all $\text{H}(\text{g})\text{-C}_{(i)}$ interactions, $i = 0, 1, \dots, 12$ are included. In particular, at the high temperature condition, the contributions to each reaction coming from both physisorption and chemisorption-type $\text{H}(\text{g})\text{-surface}$ interactions have been considered.

C. Comparison with Previous Studies. The model and conditions used in the present paper are different from those employed in previous studies on the gas-surface reaction.^{10,11,18,19} We have considered the incident atom interacting with not only the adatom but also the first-, second- and third-nearest carbon atoms surrounding the adsorption site, which can modify the overall interaction energy and open up additional channels of energy flow from $\text{H}(\text{g})$ to the surface atoms. In addition, we have also considered the propagation of the reaction energy to the distant region of the solid through both surface-layer and inter-layer carbon atoms, representing the surface relaxation effects.

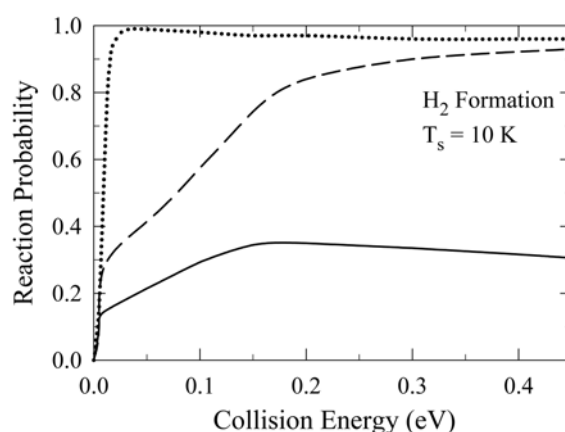


Figure 10. Comparison of the probability of $\text{H}_2(\text{g})$ formation on the collision energy. The solid curve is the present model. The dashed curve is the $b = 0$ case of the present model. The dotted curve is reproduced from Ref. 18; a smooth curve is taken from the highly oscillatory data.

To compare the results of the present study with those of others, we first calculate the collision energy dependent probability, *i.e.*, $P_{(\text{i})}(E)$ for the recombination process, where E is set to some finite value, instead of using the Maxwellian velocity (energy) distribution at a given T_g . The model is then the same as that used in all the above calculations except that the initial collision energy is fixed to E instead of the temperature T_g , *i.e.*, the same E for all 40000 trajectories. The result is shown in Figure 10 between $E = 0$ and 0.45 eV at $T_s = 10$ K (see the solid curve). Except at the lower end of E , where the collision energy is lower than the barrier height, all calculations are carried out including both contributions from the physisorption and chemisorption-type $\text{H}(\text{g})\text{-surface}$ interactions. The recombination probability is nearly constant (≈ 0.3) between $E = 0.1$ eV and 0.45 eV. This E dependence is markedly different from the values reported by Morisset *et al.*,¹⁸ which are very close to unity between $E = 0.02$ eV and 0.4 eV, see the dotted curve in Figure 10. Our values are smaller than the latter result by a factor of 2-3. Below $E = 0.01$ eV, it decreases sharply to zero. The collision model employed in the latter work is for the collinear model, where the two H atoms move on a line perpendicular to the coronene plane. Thus we set $b = 0$ in our model to mimic the latter system. As shown in Figure 10, the values of the recombination probability $P_{(\text{i})}(E)$ calculated from our $b = 0$ case in the energy range of 0.2 eV to 0.4 eV are fairly close to unity as in the calculation by Morisset *et al.*¹⁸ For example, $P_{(\text{i})}(E) = 0.910$ at $E = 0.45$ eV and it remains near 0.9 as E is lowered to 0.20 eV (see the dashed curve). When E is lowered further to 0.1 eV, the probability decreases towards ≈ 0.62 , but the latter study gives the probabilities remaining still close to unity. Below $E = 0.01$ eV both studies predict a sharp decrease in the recombination probability. This comparison shows that when the present model is applied to the collinear collision case, the result agrees fairly well with that of Morisset *et al.* at higher energies considered in Figure 10 but the discrepancy becomes significant as the collision energy is lowered. Despite

the differences at such collision energies, the principal qualitative features of the E dependence of the recombination probability on the extreme surface temperature are fairly close to each other. However, both results are very different from the values predicted by the present model of non-collinear collisions represented by the solid curve in Figure 10. The recombination probability calculated from the $b = 0$ case is always larger than that of the present model which includes all nonzero- b collisions (solid curve) as shown in Figure 10. At $E = 0.01$ eV and $T_s = 10$ K, the $b = 0$ probability is a factor of 1.5 larger. The factor is nearly 2 between $E = 0.15$ eV and 0.45 eV. A similar trend is found when the result of Morisset *et al.*¹⁸ are compared with that of the present model. Thus this comparison clearly demonstrates the important effects of nonzero- b collisions in the recombination pathway of the gas-surface reaction. When we set $b = 0$ in the high-temperature condition (1500 K, 300 K) used in Section III-A, the recombination probability is 0.511, which is nearly twice the $b \neq 0$ value 0.284.

At $E = 1500$ K, Meijer *et al.*¹¹ have calculated the $b \neq 0$ recombination probabilities 0.21 for para- H_2 and 0.26 for ortho- H_2 , the values which are somewhat smaller to our (1500 K, 300 K) value 0.284 reported above. Since the high energy tail portion of the Maxwell distribution of collision energies plays a significant role in the recombination reaction as noted in Sec. III-A, our values are expected to be larger.

Concluding Comments

The collision of gas-phase hydrogen atoms with chemisorbed hydrogen on a graphite surface has been studied using semi-classical procedures. The gas atom is considered to interact with all 13 surface-layers atoms of the three benzene-ring structure. The adatom is chemisorbed on the center site of the ring configuration, surrounded by the first-, second- and third-nearest, ..., carbon atoms in each layer. The reaction energy propagates into the bulk solid phase through vibrations involving both surface-layer and inner-layer atoms.

The recombination reaction studied is of the Eley-Rideal type in which $H(g)$ interacts directly with $H(ad)$ forming $H_2(g)$ on a subpicosecond time scale. Other reaction pathways found in the calculation are H-H exchange, collision induced desorption of $H(ad)$ without forming $H_2(g)$, and adsorption of $H(g)$ on an adjacent site with no desorption of $H(ad)$. At the temperature condition of ($T_g = 1500$ K, $T_s = 300$ K), the reaction probabilities of these four pathways are 0.284, 0.011, 0.239 and 0.005. Half the energy released in the reaction deposits in the vibrational motion of H_2 , followed by 33% in translation and 9% in rotation. Only about 8% of the energy propagates into the solid phase. Nearly 91% of $H_2(g)$ are formed when $H(g)$ approaches the region between the adatom site and the first-nearest atoms in a direct collision. The rest of H_2 are formed when $H(g)$ first approaches the second and third-nearest surface atoms in large impact parameter collisions and then steered by these atoms towards the adatom. The majority (62%) of the H_2 recombination

reaction occurs when the incident atom interacts with the surface through the chemisorption-type interaction. The rest is from the physisorption-type interaction.

At the extreme temperature environment of (10 K, 10 K), where the gas-surface interaction is considered to be the physisorption type, the extents of all probabilities are in the range of 10^{-4} . Both recombination and collision-induced desorption probabilities steadily increase to 0.06 and 0.09, respectively, as the gas temperature is raised to 100 K. On the other hand, the probabilities of exchange and adsorption reactions increase only to 0.002 and 0.006, respectively. Nearly 66% of the reaction energy deposits in the vibrational motion of H_2 but the amount of energy propagated into the surface is about 4% at (100 K, 10 K). Vibrational excitation and population inversion are significantly stronger than the high-temperature (1500 K, 300 K) case. The amount of energy deposited in translation is 16%, which is much smaller than that in the high-temperature case.

Acknowledgments. YHK gratefully acknowledges the financial support from Inha University. Computational time was supported by "the 8th Supercomputing Application Support Program" from the Korea Institute of Science and Technology Information (KISTI) and the University of Nevada Reno Chemistry Computational Program.

References

- Huber, K. P.; Herzberg, G. *Constants of Diatomic Molecules*; Van Nostrand Reinhold: New York, 1979.
- Tully, J. C. *J. Chem. Phys.* **1980**, *73*, 6333.
- Christmann, K. *Surf. Sci. Rep.* **1988**, *9*, 1.
- Jeloica, L.; Sidis, V. *Chem. Phys. Lett.* **1999**, *300*, 157.
- Van de Walle, C. G.; Street, R. A. *Phys. Rev.* **1995**, *B51*, 10615.
- Kratzer, P.; Hammer, B.; Norskov, J. K. *Phys. Rev.* **1995**, *B51*, 13432.
- Upton, T. H.; Goddard, W. A. III *Phys. Rev. Lett.* **1979**, *42*, 472.
- Nordlander, P.; Holloway, S.; Noerskov, J. K. *Surf. Sci.* **1984**, *136*, 59.
- Kratzer, P.; Brenig, W. *Surf. Sci.* **1991**, *254*, 275.
- Farebrother, A. J.; Meijer, A. J. H. M.; Clary, D. C.; Fisher, A. J. *Chem. Phys. Lett.* **2000**, *319*, 303.
- Meijer, A. J. H. M.; Farebrother, A. J.; Clary, D. C.; Fisher, A. J. *J. Phys. Chem. A* **2001**, *105*, 2173.
- Jackson, B.; Lemoine, D. *J. Chem. Phys.* **2001**, *114*, 474.
- Ghio, E.; Mattera, L.; Salvo, C.; Tommasini, F.; Valbusa, U. *J. Chem. Phys.* **1980**, *73*, 556.
- Parneix, P.; Bréchnignac, P. *Astron. Astrophys.* **1998**, *334*, 363.
- Ree, J.; Kim, Y. H.; Shin, H. K. *J. Phys. Chem. A* **2003**, *107*, 5101.
- Ree, J.; Kim, Y. H.; Shin, H. K. *Chem. Phys. Lett.* **2002**, *353*, 368.
- Sha, X.; Jackson, B.; Lemoine, D. *J. Chem. Phys.* **2002**, *116*, 7158.
- Morisset, S.; Aguilon, F.; Sizun, M.; Sidis, V. *J. Phys. Chem. A* **2004**, *108*, 8571.
- Morisset, S.; Aguilon, F.; Sizun, M.; Sidis, V. *J. Chem. Phys.* **2004**, *121*, 6493.
- Lee, S. K.; Ree, J.; Kim, Y. H.; Shin, H. K. *Bull. Korean Chem. Soc.* **2005**, *26*, 1369.
- Oh, H.-G.; Ree, J.; Lee, S. K.; Kim, Y. H. *Bull. Korean Chem. Soc.* **2006**, *27*, 1641.
- Ree, J.; Kim, Y. H.; Shin, H. K. *J. Chem. Phys.* **1996**, *104*, 742.
- Blanco, A.; Fonti, S.; Muci, A. M.; Orofino, V. *Astrophys. J.* **1996**, *472*, 419.

24. Kroto, H. W.; Heath, J. R.; O'Brien, S. C.; Curl, R. F.; Smalley, R. E. *Astrophys. J.* **1987**, 314, 352.
 25. Sofia, U. J.; Cardelli, J. A.; Savage, B. D. *Astrophys. J.* **1994**, 430, 650.
 26. Guillois, O.; Ledoux, G.; Nenner, I.; Papoular, R.; Reynaud, C. *Faraday Discuss.* **1998**, 109, 335.
 27. Küppers, J. *Surf. Sci. Rep.* **1995**, 22, 249.
 28. Lamoén, D.; Persson, B. N. J. *J. Chem. Phys.* **1998**, 108, 3332.
 29. Lang, L.; Doyen-Lang, S.; Charlier, A.; Charlier, M. F. *Phys. Rev. B* **1994-II**, 49, 5672.
 30. Sidis, V.; Jeloaiica, L.; Borisov, A. G.; Deutscher, S. A. In *Molecular Hydrogen in Space*; Combes, F.; Pineau des Forêts, G., Eds.; Cambridge Univ. Press: 2000; pp 89-98.
 31. Morisset, S.; Aguillon, F.; Sizun, M.; Sidis, V. *Phys. Chem. Chem. Phys.* **2003**, 5, 506.
 32. Mizushima, M. *The Theory of Rotating Diatomic Molecules*; Wiley: New York, 1975.
 33. Dinger, A.; Lutterloh, C.; Biener, J.; Küppers, J. *Surf. Sci.* **1999**, 421, 17.
 34. Adelman, S. A. *J. Chem. Phys.* **1979**, 71, 4471.
 35. *American Institute of Physics Handbook*, 3rd ed.; Gray, D. E., Ed.; McGraw-Hill: New York, 1972; section 4, p 115.
 36. Kim, Y. H.; Ree, J.; Shin, H. K. *J. Chem. Phys.* **1998**, 108, 9821.
 37. Eenshuijstra, P. J.; Bonnie, J. H. M.; Los, J.; Hopman, H. J. *Phys. Rev. Lett.* **1988**, 60, 341.
 38. Jackson, B.; Persson, M. *J. Chem. Phys.* **1995**, 103, 6257.
 39. Shin, H. *Chem. Phys. Lett.* **1995**, 244, 235.
 40. Polanyi, J. C.; Tardy, D. C. *J. Chem. Phys.* **1969**, 51, 5717.
 41. Polanyi, J. C. *Acc. Chem. Res.* **1972**, 5, 161.
 42. Kolos, W.; Szalewicz, K.; Monkhorst, H. J. *J. Chem. Phys.* **1986**, 84, 3278.
 43. Kolos, W.; Wolniewicz, L. *J. Chem. Phys.* **1968**, 49, 404.
 44. Gould, R. J.; Salpeter, E. E. *Astrophys. J.* **1963**, 138, 393.
 45. Black, J. H.; Dalgarno, A. *Astrophys. J.* **1976**, 203, 132.
 46. Duley, W. W.; Williams, D. A. *Interstellar Chemistry*; Academic Press: London, 1984.
 47. Ree, J.; Kim, Y. H.; Shin, H. K. *Chem. Phys. Lett.* **2002**, 353, 368.
 48. Ko, Y.; Ree, J.; Kim, Y. H.; Shin, H. K. *Bull. Korean Chem. Soc.* **2002**, 23, 1737.
-